Paper

Heavy Ion Beam Illumination Uniformity in Heavy Ion Beam Inertial Confinement Fusion

Tetsuo Someya* Non-member
Aleksandar Ogoyski* Non-member
Shigeo Kawata* Member
Toru Sasaki* Non-member

In heavy ion beam (HIB) inertial confinement fusion (ICF), key issues include an accelerator design for an intense HIB, an efficient HIB transport, interaction between HIB and reactor gas, a HIB-target interaction, a reactor design and so on. In this paper, three-dimensional computer simulations are performed for a HIB irradiation onto a direct-driven spherical fuel pellet in HIB ICF in order to clarify the dependence of multi-HIB illumination non-uniformity on parameter values of HIB illumination. We investigate the energy deposition non-uniformity using 12, 20, 32, 60, 92 and 120-beam irradiation systems. In this study, effects of HIB temperature and emittance are also evaluated. The calculation results demonstrate that we can realize a sufficiently low non-uniform energy deposition, for example, less than 2[%] even for a 32-beam irradiation system using the Gaussian beam.

Keywords: stopping power, heavy ion beam, inertial confinement fusion, non-uniformity

1. Introduction

Key issues in heavy ion beam (HIB) inertial confinement fusion (ICF) include an accelerator design for intense HIBs, efficient HIB transport, a HIB-target interaction, a reactor design and so on [(1)~(5)]. In this study, we focus on a HIB-target interaction in ICF. In HIB ICF, the beam irradiation non-uniformity on a direct-driven fuel pellet must be suppressed under a few % in order to achieve a symmetric fuel pellet implosion [(6)~(10)]. Therefore a multi-HIB illumination is required to achieve a low beam non-uniformity in the pellet implosion. On the other hand, the total HIB number should be restricted to a realistic number, for example, less than a few hundred beams. Therefore, in this study, we simulate a HIB illumination on the spherical direct-driven target using 12, 20, 32, 60, 92 and 120-beam irradiation systems. In Section 2 we present a detail of beam illumination.

The HIB illuminates the spherical target and deposits its energy on the target. We calculate the deposition energy on the spherical target according to a stopping power [(11)~(18)]. We also show the detail of stopping power in Section 2. The main purpose of this study is to clarify the multi-HIB energy deposition non-uniformity onto a direct-driven spherical pellet. The HIB ions impinge the target surface, penetrate relatively deep into the deposition layer and deposit their energy in a rather wide region in the deposition layer: this HIB deposition feature influences the beam illumination non-uniformity. The HIB temperature and emittance effects are also evaluated. We also study the effect of the total HIB number on the HIB illumination non-uniformity. For the evaluations of the illumination non-uniformity on the target, we compute the root mean square (RMS) and the peak to valley (PTV) non-uniformities on the target [(19)]. In addition, we perform mode analyses of the HIB deposition energy on the spherical fuel target.

* Department of Energy and Environmental Science, Utsunomiya University
Yohtoh 7-1-2, Utsunomiya 321-8585

2. Simulation Model

In this study, we use a lead (Pb^+) beam as a HIB in ICF. The beam parameters are as follows: the mean particle energy is 8.0 [GeV], the maximal initial beam density is 1.3×10^{11} [1/cm^3]. The HIB radius varies from 2.7 to 3.8 [mm] on the pellet surface depending on the beam temperature and emittance. For example, the beam radius is 3.0 [mm] at the pellet surface in the case of a zero-temperature beam. In this study, we select two types of HIB transverse number density profiles: the Kapchinskij-Vladimirskij (K-V) and the Gauss distributions with the Maxwell-distributed particle energy with the beam longitudinal temperature of 100 [MeV]. The Gaussian distribution is shown in Eq. (1).

$$n(r) = \frac{1}{\sqrt{2\pi\sigma^2}} \exp\left(-\frac{r^2}{2\sigma^2}\right) \cdots\cdots\cdots\cdots\cdots\cdots (1)$$

Here, $n(r)$ is a number density as a function of beam radius r. The σ is standard deviation. In this study the standard deviation is equal to the 1.2 times of the beam radius on the pellet surface.

2.1 Stopping Power The HIB energy deposition comes mainly from the Coulomb collisions between bound/free electrons and beam ions. The Coulomb

collisions between beam ions and target ions, nucleus scattering and the plasma wave excitation contribute the stopping power. The ion stopping power of the target is considered to be the sum of the energy deposited in a target nuclei, target bound and free electrons, and target ions [14]: $E_{stop} = E_{nuc} + E_{free} + E_{bound} + E_{ion}$, where E_{stop} is the deposition energy in the target, E_{nuc} is the deposition energy by the nucleus scattering, E_{free} is by the free electron, and E_{ion} is by the target ion. The nucleus stopping power E_{nuc} becomes effective at the end of the stopping range and describes the elastic collisions between the projectile ions and target nuclei [11] [20]. When the target temperature rises and the target is ionized, free electrons contribute the stopping power, through the Coulomb collisions and the plasma collective wave excitations. The free electron stopping power E_{free} is calculated by the Coulomb collision between projectile ions and the target free electrons [17] [18]. E_{ion} is evaluated by the Coulomb collisions between HIB particles and target ions. The Linhard and Bethe-Bloch equations describe the bound electron stopping power E_{bound}. We use the Bethe equation to calculate the bound electron stopping power at the high beam energy region in this study [16]. In the middle beam energy region, we calculate the bound stopping power from the Bethe equation with the shell correction [11]. At low beam energies, the stopping power theory is mostly evaluated by the Thomas-Fermi model of the atom [11] [12] [20]. Therefore we use the LSS equation at the low beam energy domain to calculate the bound electron stopping power [11].

2.2 Beam Illumination Scheme In this study, we simulate a multi-HIB illumination on a spherical target using 12, 20, 32, 60, 92 and 120-beam irradiation systems. Each beam position is decided as follows: in the 12-beam system each beam center coincides with the center of each face at the regular dodecahedron. In the same way the 20-beam system is based on the regular icosahedron. We employ the 32-beam system shown by Skupsky [8]. The 60-beam system is vertices of a soccer ball or fullerene [6] [7]. The 92-beam system is combination of 12, 20, and 60-beam systems. The 120-beam system is the combination of two 60-beam systems, each of which is shifted by 90 degree in the vertex direction.

2.3 Beam Particle Orbit in the Target In our study we select two types of target: one is an Al mono-layer pellet structure with the 4-mm external radius as shown in Fig. 1 a) and another one is a Pb+Al pellet structure [4] with the same external radius as shown in Fig. 1 b). In the latter pellet structure, the outer Pb layer thickness and mass density are 0.03 [mm] and 11.3 [g/cm^3], respectively. The Al layer thickness and mass density are 0.97 [mm] and 2.69 [g/cm^3], respectively.

In order to calculate the beam particle orbit we define the beam particle position (R, Θ, Φ) at the tangential target surface and the focal position (f, Θ_f, Φ_f) as shown in Fig. 2a). Then we can calculate the beam particle orbit in the target (r, θ, ϕ) by Eq. (2) using the target radius r.

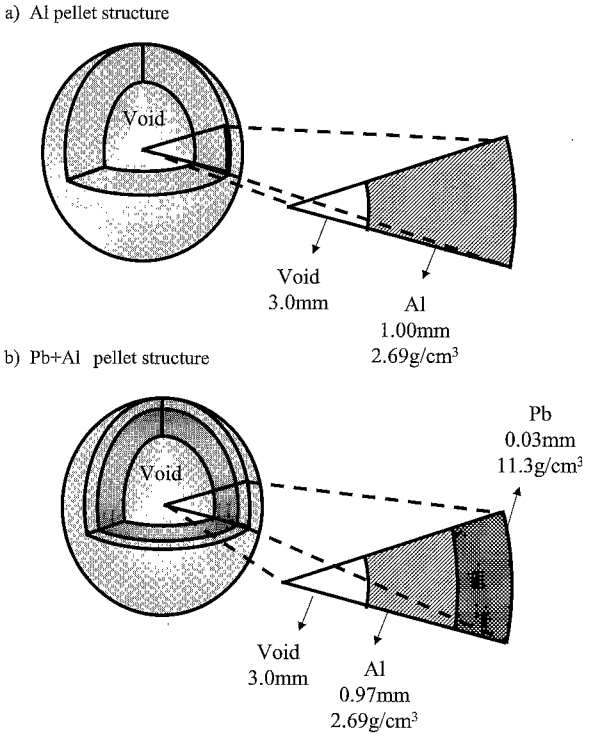

Fig. 1. Fuel target structure: a) the Al layer thickness and mass density are 1.00mm and 2.69g/cm^3, respectively, b) the Pb layer thickness and mass density are 0.03mm and 11.3g/cm^3, and the Al layer thickness and mass density are 0.97mm and 2.69g/cm^3, respectively

$$\frac{r\sin\theta\cos\phi - R\sin\Theta\cos\Phi}{f\sin\Theta_f\cos\Phi_f - R\sin\Theta\cos\Phi} = \frac{r\sin\theta\sin\phi - R\sin\Theta\sin\Phi}{f\sin\Theta_f\sin\Phi_f - R\sin\Theta\sin\Phi} = \frac{r\cos\theta - R\cos\Theta}{f\cos\Theta_f - R\cos\Theta} \quad \cdots\cdots (2)$$

By Eq. (2) we can calculate the beam orbit, i.e. (r, θ, ϕ).

2.4 Beam Divergence The beam particle may slightly diverge by a finite emittance in the transverse direction. Therefore we include a beam emittance effect and change the beam radius not to miss the target so that all ions hit the target surface. In Fig. 2b), we define a relation between a beam transverse emittance and a divergence angle α_{dvr}. R_{en} is the beam radius at the fusion reactor wall, R_{ch} is the reactor radius, f is the focal length between the beam focal position and the target center, R_f is the focal spot radius, and R_{beam} is the beam radius at the target surface (see Fig. 2b)). The beam divergence angle α_{dvr} is defined as follows:

$$\alpha_{dvr} = \frac{\epsilon_r}{R_{en}} \quad \cdots\cdots (3)$$

Here, ϵ_r is a beam transverse emittance. In this study, we calculate a beam divergence angle from the beam transverse emittance . The beam transverse emittance is 5.0 [mm-mrad] in this study. From Eq. (3), the beam divergence angle α_{dvr} is calculated to be about 8.2×10^{-3} degree in the case of ϵ_r=5.0 [mm-mrad] and

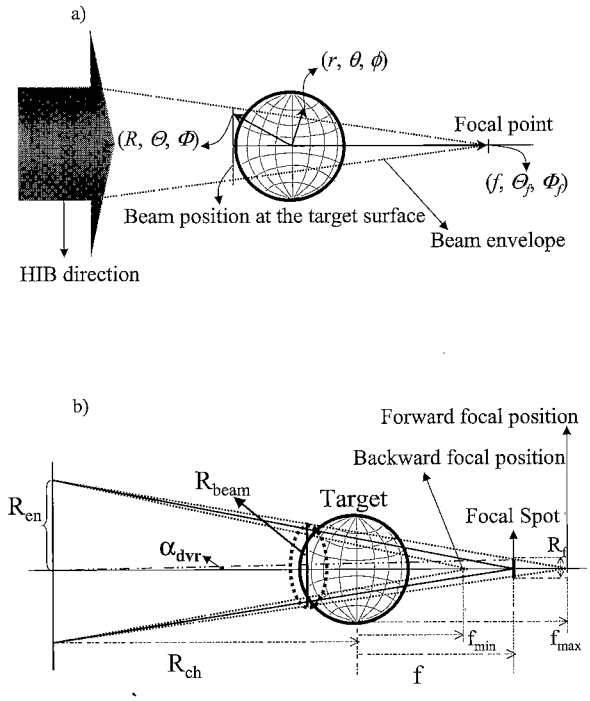

Fig. 2. a) Beam focal spot and target pellet; (R, Θ, Φ) means the beam particle position at the tangential target surface, (f, Θ_f, Φ_f) is the focal position and (r, θ, ϕ) is the beam particle position in the target, b) the relationship between a beam emittance and a divergence angle at the beam port; R_{en} is a chamber radius of a fusion reactor, R_{ch} is the reactor radius, f is the beam focal spot lengt from the target center, R_f is the focal spot radius, $\alpha_{dvr}$is a beam divergence angle, and R_{beam} is the beam radius at the tangential target surface

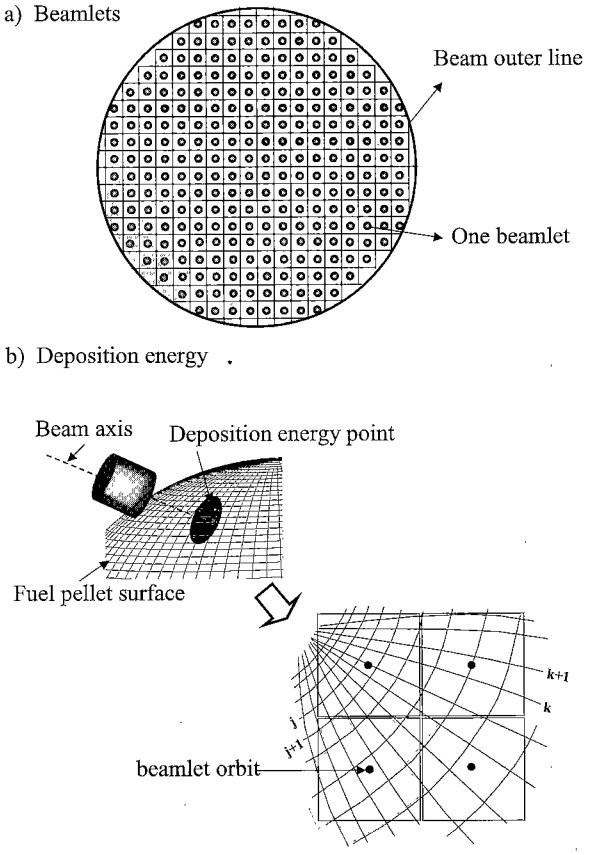

Fig. 3. a) Beamlet. Each beamlets deposit its energy in the spherical target, b) the beamlet has an effective area. The deposition energy at a mesh point is calculated by using the beamlet effective area

R_{en}=35 [mm]. In our study the relation between the focal length f and the beam radius R_{beam} is defined by

$$f = \frac{R_{beam}R_{ch} - R_p R_{en}}{R_{en} - R_{beam}} \cdots\cdots (4)$$

In addition, the beam focal position moves backward and forward by the beam divergence angle as shown in Fig. 2b). Therefore we use Eqs. (5) and (6) to calculate the backward and forward focal position.

$$f_{\min} = R_{en}\tan\left(\xi - 0.07145\alpha_{dvr}\right) - R_{ch} \cdots\cdots (5)$$

$$f_{\max} = R_{en}\tan\left(\xi + 0.07145\alpha_{dvr}\right) - R_{ch} \cdots\cdots (6)$$

Here, $f_{\min}$ is the backward focal position of the beam focal spot, $f_{\max}$ is the forward focal position, and ξ is given by $\xi = a\tan[(R_{ch} + f)/R_{en}]$. From Eqs. (4), (5) and (6) the beam radius at the fuel pellet surface changes 2.7 [mm] to 3.8 [mm] in the case of 5.0 [mm-mrad] emittance, so that any HIB ions do not miss impinging the pellet surface.

2.5 Deposition Energy Calculation Procedure

In this study, we divide one HIB into 316 beamlets in order to simulate a precise HIB illumination non-uniformity as shown in Fig. 3a). Each beamlet deposits its energy on space meshes of the spherical target as shown in Fig. 3b). Then in order to calculate the deposition energy in one mesh, we use Eq. (7).

$$E_{stop} = \frac{dE}{dl} V n^{2/3} \cdots\cdots (7)$$

Here, dE/dl is the stopping power, that is, a beamlet deposition energy per unit length, n is the beam particle number density, and V is the volume of one cell in the target.

The deposition energy is distributed to the mesh points. Each beamlet has an effective area, and the deposition energy is distributed to the meshes by the beamlet effective area as shown in Fig. 3b). When multi-HIBs illuminate the spherical target and deposit their energy on the target, the deposition energy is calculated by Eq. (8)

$$E_{ijk} = \sum_N E_{stop} \cdots\cdots (8)$$

Here, E_{ijk} is the deposition energy at each mesh point denoted by (i, j, k) in the 3-dimensional space and N is the number of HIBs impinging the cell.

2.6 Evaluation of Non-uniformity on Spherical Target In this study, we evaluate the energy non-uniformity at the target. In ICF, the beam irradiation non-uniformity on the fuel target must be suppressed

under a few % in order to achieve a symmetric fuel pellet implosion [6]~[10]. In HIB ICF the Bragg peak deposition area plays the most important role for a target implosion. Therefore we define the total relative root-mean-square (RMS) as follows:

$$\sigma_{RMS} = \sum_{i}^{n_r} w_i \sigma_{RMS_i} \quad \cdots\cdots (9)$$

$$\sigma_{RMS_i} = \frac{1}{\langle E \rangle_i} \sqrt{\frac{\sum_{j}^{n_\theta} \sum_{k}^{n_\phi} \left(\langle E \rangle_i - E_{ijk} \right)^2}{n_\theta n_\phi}} \quad \cdots\cdots (10)$$

$$w_i = \frac{E_i}{E} \quad \cdots\cdots (11)$$

The peak-to-valley (PTV) non-uniformity is defined as follows:

$$\sigma_{PTV} = \sum_{i}^{n_r} w_i \sigma_{PTV_i} \quad \cdots\cdots (12)$$

$$\sigma_{PTV_i} = \frac{E_i^{\max} - E_i^{\min}}{2\langle E \rangle_i} \quad \cdots\cdots (13)$$

Here, σ_{RMS_i} and σ_{PTV_i} are the RMS and PTV non-uniformities on the i-th surface of deposition, respectively. w_i is the weight function in order to include the Bragg peak effect or the deposition profile. n_r, n_θ and n_ϕ are mesh numbers in each direction of the spherical coordinate. $\langle E \rangle_i$ is the mean deposition energy on the i-th surface, E_i is the total deposition energy on the i-th surface, and E is the total deposition energy. $E_i^{\max}$ and $E_i^{\min}$ are the maximal and minimal deposition energies on the i-th surface, respectively.

3. Simulation Results

Figure 4a) shows the deposition energy of beam particles at each surface without the beam temperature effect for Al layer target with the chamber radius of 5 [m], 120-beam system, and the K-V distribution. In Fig. 4a), we can see the Bragg peak at the middle layer of the energy absorption layer, and the RMS and PTV non-uniformities are low at the Bragg peak layer. The total RMS non-uniformity is evaluated by Eq. (9), and the result is σ_{RMS}=4.44 [%]. Figure 4b) shows the energy deposition in the case of 120-beam system, 5 [m] chamber radius, the K-V distribution and the Al only target including the longitudinal beam temperature of 100 [MeV] and the transverse beam radial emittance of 5 [mm-mrad]. In this case the mean HIB particle energy is 8 [GeV]. We can see that the Bragg peak moves slightly outward in the radial direction and the RMS non-uniformity becomes σ_{RMS}=1.52 [%]. The HIB illumination non-uniformity in the realistic case including the beam temperature or the beam divergence becomes small compared with that in the case with the zero-temperature HIB. This result presents that the HIB illumination non-uniformity can be smoothed and suppressed due to the effects of the beam temperature and the transverse emittance.

We also calculate the deposition-energy spectra at the

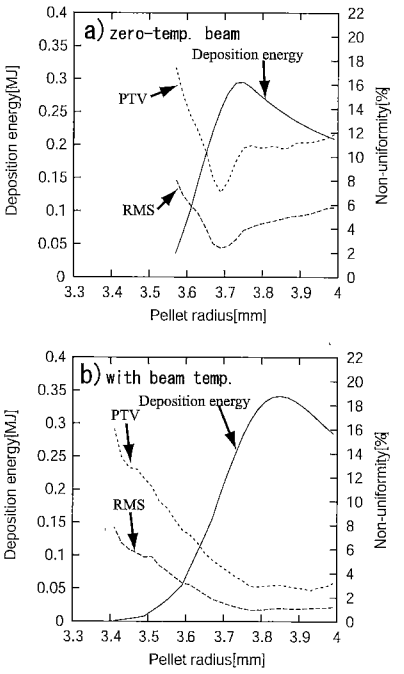

Fig. 4. The deposition energy of beam particles at each surface in the case of Al layer target with the chamber radius of 5m, 120-beam system, and the K-V distribution for the cases a) without the beam temperature effect and b) with the temperature effect

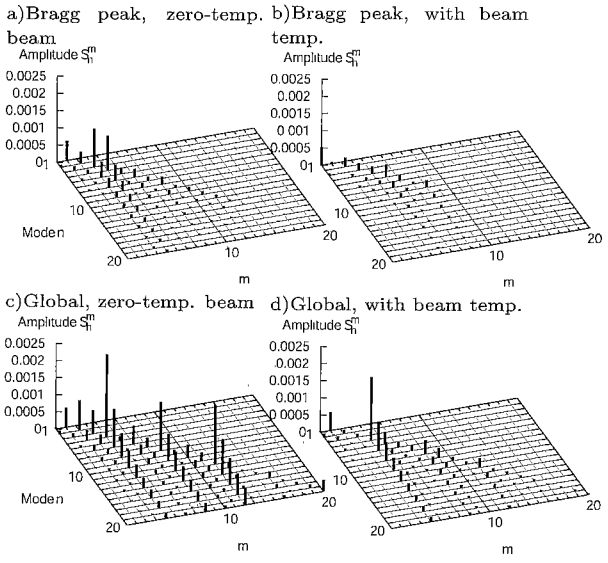

Fig. 5. The energy-spectra at the Bragg peak layer a) for the zero-temperature beam (r=3.73 [mm]) and b) with the beam temperature of 100 [MeV] (r=3.83 [mm]); Figures c) and d) shows the global non-uniformity spectra using the weight w_i for the zero-temperature beam and with the beam temperature of 100 [MeV]

Bragg peak layer for the zero-temperature beam (r=3.73 [mm]) and for the case with the beam temperature of 100 [MeV] (r=3.83 [mm]) as shown in Figs. 5a) and 5b). Figures 5c) and 5d) are the global non-uniformity spectra using the weight w_i for the zero-temperature beam and

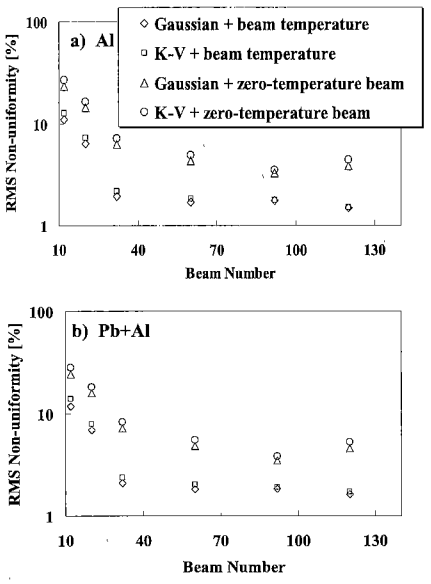

Fig. 6. The RMS non-uniformity versus the HIB total number in the cases of a) Al layer target and b) Pb+Al layer target with the chamber radius of 5; the marked diamonds, triangles, squares, and circles mean the results in the cases of the Gauss distribution with and without the temperature effect, and of the K-V distribution with and without the temperature effect, respectively

for the case with the beam temperature of 100 [MeV]. In Fig. 5, $(n,\ m)$, and S_n^m are the mode numbers and the amplitude of spectrum, respectively. If the deposition energy is distributed in a perfect spherical symmetric way, the amplitude of spectrum is set to 1.0 for the mode (n, m)=(0, 0) in our study. In order to achieve a symmetric energy deposition in the direct-drive HIB ICF, the most spectra should be concentrated on the mode (n, m)=(0, 0), and the amplitude of the mode (n, m)=(0 0) has a large value near 1.0 in our simulation results, compared with those for other modes. For this reason, in this paper, we focus on the amplitudes of spectrum modes except the mode (n, m)=(0, 0). Therefore our calculation results in Fig. 5 present the spectra without the mode of (n, m)=(0, 0). In Fig. 5 the amplitudes of the spectra at the Bragg peak layer is small compared with those for the global non-uniformity. This result means that the deposition energy at the Bragg peak layer is more uniform compared with other layers. In HIB ICF the Bragg peak area plays an important role on the symmetric target implosion. Therefore we expect that we can realize an effective compression of target and efficient target implosion. We also confirm that the amplitude in the case including the beam temperature becomes small compared with that in the case of the zero beam temperature, as expected by the results presented above. Moreover in Figs. 5a) and b) the amplitude of the deposition-energy spectrum at the mode (n, m)=(0, 0) is 0.97 in the case with the zero beam temperature, and the amplitude of the energy spectrum at the mode (n, m)=(0, 0) is 0.99 in the case including the beam temperature.

Figure 6 shows the RMS non-uniformity versus the HIB total number in the cases of a) Al layer target and b) Pb+Al layer target with the chamber radius of 5 [m]. The marked diamonds, triangles, squares, and circles mean the results in the cases of the Gauss distribution with and without the temperature effect, and of the K-V distribution with and without the temperature effect, respectively. Particularly, in the case with the Gaussian distribution with the beam temperature of 100 [MeV] marked by diamonds in Fig. 6, the RMS non-uniformity is 1.49 [%] for Al structure and 1.63 [%] for Pb+Al structure. These values are small compared with those in the K-V distribution with the beam temperature (1.52 [%] for Al structure and 1.72 [%] for Pb+Al structure in the case of 120-beam system). Therefore our calculation results demonstrate that the more realistic beam, that is, the Gaussian beam may be useful for HIB ICF in order to achieve a symmetric implosion.

4. Conclusions

In this paper, we studied the HIB deposition non-uniformity in a direct-driven HIB-ICF pellet. We also included the effect of a beam longitudinal temperature and the beam transverse emittance. From our simulation results, we confirm that the HIB illumination RMS non-uniformity is 1.49 [%]in the case of the Al monolayer structure target, with the beam temperature of 100 [MeV], the 120-beam system and the Gaussian beam. In the case of the Pb+Al target structure, the RMS non-uniformity is 1.63 [%]. From these results, we expect that the fuel may be successfully imploded and the fusion energy can be released from the direct-driven fuel pellet in HIB ICF.

In order to investigate a dynamic HIB illumination non-uniformity, hydrodynamic implosion simulations coupled with our 3-D HIB illumination code should be performed, and this work should be done in the near future as well as the displacement of target position in a fusion reactor.

Acknowledgment

This work is partly supported by the JSPS(Japan Society for the Promotion of Science). We would like also to present our thanks to colleauges in the Japan and US HIF research groups for their fruitful discussions on this subject.

(Manuscript received June 18, 2003)

References

(1) W. J. Hogan, R. Bangerter, and G. L. Kulcinski: "Energy from inertial fusion", *Phys. Today*, Vol.45, pp.42-50 (1992)

(2) M. Tabak and D. Callahan-Miller: "Design of a distributed radiator target for inertial fusion driven from two sides with heavy ion beams", *Phys. Plasmas*, Vol.5, pp.1895-1900 (1998)

(3) D. A. Callahan: "Interactions between neighboring beams in a heavy ion fusion reactor chamber", *Appl. Phys. Lett.*, Vol.67, pp.3254-3256 (1995)

(4) J. Sasaki, T. Nakamura, Y. Uchida, T. Someya, K. Shimizu, M. Shitamura, T. Teramoto, A. Blagoev, and S. Kawata: "Beam non-uniformity smoothing using density valley formed by heavy ion beam deposition in inertial confinement fusion fuel pellet", *Jpn. J. Appl. Phys.*, Vol.40, pp.968-971 (2001)

(5) D. R. Welch, D. V. Rose, B. V. Oliver, T. C. Genoni, and R. E. Clark, C. L. Olson, and S. S. Yu: "Simulations of intense heavy ion beams propagating through a gaseous fusion target chamber", *Phys. Plasmas*, Vol.9, pp.2344-2353 (2002)
(6) M. Murakami: "Irradiation system based on dodecahedron for inertial confinement fusion", *Appl. Phys. Lett.*, Vol.27, pp.1587-1589 (1995)
(7) M. Murakami, K. Nishihara, and H. Azechi: "Irradiation nonuniformity due to imperfections of laser beams", *J. Appl. Phys.*, Vol.74, pp.802-808 (1993)
(8) S. Skupsky and K. Lee: "Uniformity of energy deposition for laser driven fusion", *J. Appl. Phys.*, Vol.54, pp.3662-3671 (1983)
(9) S. Kawata and K. Niu: "Effect of nonuniform implosion of target on fusion parameters", *J. Phys. Soc. Jpn.*, Vol.53, pp.3416- (1984)
(10) M. H. Emery and J. H. Gardner: "Hydrodynamic target response to an induced spatial incoherence-smoothed laser beam", *Phys. Fluids* B, Vol.3, pp.2640-2651 (1991)
(11) H. H. Andersen and J. F. Ziegler: The Stopping and Ranges of Ion in Matter, Vol.3, Pergamon Press (1977)
(12) F. C. Young, D. Mosher, S. J. Stepanakis, S. A. Goldstein, and T. A. Mehlhoen: "Measurements of enhanced stopping of 1-MeV deuterons in target-ablation plasmas", *Phys. Rev. Lett.*, Vol.49, pp.549-553 (1982)
(13) K. A. Long and N. A. Tahir: "Range shortening, radiation transport, and Rayleigh-Taylor instability phenomena in ion-beam-driven inertial-fusion-reactor-size targets: implosion, ignition, and burn phases", *Phys. Rev. A*, Vol.35, pp.2631-2659 (1987)
(14) T. A. Mehlhorn: A finite material temperature model for ion enrgy deposition in ion driven ICF target, Sandia National Laboratories, SAND80-0038 (1980)
(15) J. A. Swegle: Beam and deposition stability in light ion fusion targets, Sandia National Laboratories, SAND82-0072 (1982)
(16) T. A. Mehlhorn, J. M. Peek, E. J. Mcguire, J. N. Olsen, and F. C. Young: Current status of calculations and measurements of ion stopping power in ICF plasmas, Sandia National Laboratories, SAND83-1519 (1983)
(17) T. Peter and J. M. Vehn: "Energy loss in dense plasma. I. Linear and nonlinear Vlasov theory for stopping power", *Phys. Rev. A*, Vol.43, pp.1998-2014 (1991)
(18) T. Peter and J. M. Vehn: "Energy loss of heavy ions in dense plasma. II. Noneequilibrium charge states and stopping powers", *Phys. Rev. A*, Vol.43, pp.2015-2030 (1991)
(19) M. Murakami and J. M. Vehn: "Radiation symmetrization in indirectly driven ICF targets", *Nucl. Fusion*, Vol.31, pp.1333-1341 (1991)
(20) P. Wang, T. M. Mehlhorn, and J. J. MacFarlane: "A unified self-consistent model for calculating ion stopping power in ICF plasma", *Phys. Plasmas*, Vol.5, pp.2977-2987 (1998)

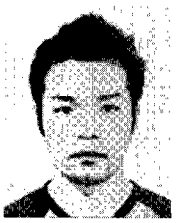

Tetsuo Someya (Non-member) received B. E. and M. S. degrees from the Department of Energy and Environmental Science, Utsunomiya University, Tochigi, Japan in 2001 and 2003. He has been interested in energy problem, heavy ion beam (HIB)inertial confinement fusion (ICF), and beam final transport in HIB ICF.

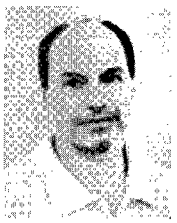

Alaksandar Ogoyski (Non-member) received Ph. D. from Sofia University, Bulgaria in 1999. From October 2001, with the support of JSPS, became a postdoctoral researcher at the department of Electrical and Electronic Engineering, Utsunomiya University, Tochigi, Japan. He has been interested in the inertial confinement fusion, stopping power, and high energy physics.

Shigeo Kawata (Member) recieved Ph.D from Tokyo Institute of Technology(TIT), Tokyo, Japan in 1985. In 1981 he became a research associate in Dept. of Energy Sciences, TIT, in 1986 he became an associate professor in Nagaoka Univ. of Tech. and in 1999 he became a professor in Utsunomiya Univ. He has been interested in inertial confinement fusion, energy problem, computational physics, and computer-assisted problem solving environment.

Toru Sasaki (Non-member) received B. E. from Department of Electrical and Engineering, Utsunomiya University, Tochigi, Japan in 2003. He has been interested in HIB ICF.